OPEN ACCESS Freely available online

IJCMB
International Journal of Clinical Medicine and Bioengineering

ISSN 2737-534X
Volume 2, Issue 1
https://www.iikii.com.sg/journal/IJCMB
International Journal of Clinical Medicine and Bioengineering

Article

Analysis of Vortex-Generation Using Adaptive Finite Element Method to Simulate Hemodynamics of Sigmoid Sinus Diverticulum

Hui-Fang Lin and Yi-Chern Hsieh *

Department of Power Mechanical Engineering, National Formosa University, Taiwan; d0675102@gm.nfu.edu.tw
* Correspondence: ych@nfu.edu.tw; Tel.: (+88656315419.)

Received: Feb 3, 2022; **Accepted:** Mar 3, 2022; **Published:** Mar 30, 2022

Abstract: In various practical physical problems, the formation of the vortical flow inside the flow field has different effects and consequences. The diverticular vortex has been considered one of the causative factors of venous pulsatile tinnitus (PT). Thus, we aimed to solve the diverticular vortex by using the adaptive finite element method. We investigated the physical phenomena of the diverticular flow field generated during the cardiac cycles and transient changes of various physical phenomena before and after the vortex. The three-dimensional (3D) computational reconstructive geometry was created by combining computed-tomography images using MIMICS 19.0 software. Flow field calculation was performed with the software COMSOL 5.6 by implementing the 3D unsteady k-ω turbulent model. The results showed that the overall state of blood flow in the sigmoid sinus and the pressure in the diverticulum changed secondarily to the cardiac cycles. Before the vortex was generated inside the diverticulum, the magnitude and the fluctuation of the inertial force in all directions become larger than those in regions without a vortex. After the appearance of the vortex, the fluctuation of its inertial force tended to be moderate at different points, and the results were similar to those regions without a vortex. The calculation of error estimates in this study met convergence, and different time intervals also exhibited expected results. The study result provides a basis for understanding the effect and cause prior to the vortex generation on venous PT.

Keywords: Adaptive, Finite element method, Vortex, Turbulent flow, Diverticulum, Venous pulsatile tinnitus

1. Introduction

At present, venous pulsatile tinnitus (PT) is a common source of objective tinnitus. PT is synchronous with the cardiac pulse, and the harmonic range of PT is generally less than 1500 Hz [1]. Tinnitus affects the patient's subjective psychological state. In subjects with objective tinnitus, the sigmoid sinus wall anomalies or vibration of middle ear muscles are detected through radiological imaging techniques or an otoscope, whereas the phantom perception of sound due to hearing loss or stress is the primary cause of subjective tinnitus [2]. For example, vascular PT, a common form of objective tinnitus, results from hemodynamic alterations in the blood vessels of the brain and head, and neck. The generated flow noise is then transmitted to the cochlea. In addition, vascular PT causes tinnitus due to abnormal changes in the shape of anatomical structures of the temporal bone. Clinical characteristics of different types of vascular PT and their clinical presentations have been described [3–5]. Computational fluid dynamics (CFD) has become indispensable for the recent hemodynamic, acoustic, and otomechanic research of PT [6,7]. In this study, the 3D geometry of the transverse-sigmoid sinus and the calculation of the sinus flow field were investigated with the setup of transient flow velocity. Then, the software COMSOL 5.6 (COMSOL AB, Stockholm, Sweden) was used for the computation of the flow field. The adaptive finite element theory was applied to the calculation of space [8] and time [9].

In this study, we delved into the generation of the diverticular vortex of a subject with venous PT. The vortex at the sigmoid sinus diverticulum is typically the physical phenomenon before and after the quantifying generation of the vortex. To understand these phenomena, we first expatiated the vortical flow structures and the concept of vortex dynamics by mainly using the coherent structure of space and the evolution of time. For example, Jeong et al. conducted a plethora of in-depth research on vortex and regarded to understand if an instantaneous vortex improves the completeness of vortex structural dynamics [10]. Discontinuous vortices are found in a variety of flow conditions as they are generated near the saddle point and then develop into the center of the coherent structure. The disintegration and reorganization process of the coherent structure is the main cause of the noise, not the pairing of the vortex [10]. This research applied the previous philosophical concepts of adaptive computing [11]. With the help of computing software, CFD calculations were carried out without increasing the computational workload while simultaneously

retaining results with reasonable precision. The knowledge of vortex generation provides the theoretical basis for the pathophysiology insights of venous PT.

2. Theoretical Basis

The theoretical basis of scientific computing is derived from the calculation results of space segmentation and the estimation of error size in the future. Then, it is decided whether to continue to increase the amount of calculation to improve the accuracy of the calculation. After the determination of the space, the segmentation state is completed. The calculation of the time interval can be performed to reduce the calculation results due to the time interval and minimize the amount of calculation and the calculation error at the same time. The basic theory is described as follows.

To describe the main physical problems of this study, the following equations are used as a modeling method.

$$u_t + (u \cdot \nabla)u - \nabla \cdot \sigma(u, p) = f \text{ in } \Omega \times [0, T] \quad (1)$$

$$\nabla \cdot u = 0 \text{ in } \Omega \times [0, T] \quad (2)$$

The generalized boundary conditions are expressed with the following three equations.

$$\mathbf{u} = \mathbf{g} \text{ on } \partial\Omega_D \times [0, T] \quad (3)$$

$$\boldsymbol{v}_{\nabla \boldsymbol{u}} \cdot \mathbf{n} - p_n = 0 \text{ on } \partial\Omega_N \times [0, T] \quad (4)$$

$$\mathbf{u}(\boldsymbol{x}, 0) = \boldsymbol{u}_0(\boldsymbol{x}) \text{ in } \Omega \quad (5)$$

The above are the governing equations to be applied to calculate this research problem. To omit the description of the functional background, constraints, and restricted categories of relatively pure applied mathematics, the calculation are based on the calculation method of the post-period error estimation in the adaptive calculation. Therefore, only from engineering, the outline of the problem is from a computational point of view. The problem dealt with in this paper was based on the requirement of a theoretical foundation and discussed from the perspective of spatial error. Therefore, the three-dimensional Newtonian fluid with steady-state viscosity and incompressibility, and its physical properties are expressed by the equation module as follows.

$$(\mathbf{u} \cdot \nabla)\mathbf{u} - \nabla \cdot \boldsymbol{\sigma}(\mathbf{u}, p) = \mathbf{f} \text{ in } \Omega \quad (6)$$

$$\nabla \cdot \mathbf{u} = 0 \text{ in } \Omega, \ u = 0 \text{ on } \partial\Omega \quad (7)$$

The above two equations are the continuity equation and Navier-Stokes equations respectively, where $\mathbf{u}=\mathbf{u}(\mathbf{x})$ is the velocity field of the fluid, $\mathbf{x} = (x_1, \ldots, x_n) \in \Omega$ is the position coordinate. For $\Omega \subset \mathbf{R}^n$, n = 3 in this study, refering to the field of computing. $\partial\Omega$ refers to the Lipschitz boundary of the computational domain. ∇ is the well-known del vector operator. $\boldsymbol{\sigma}(\mathbf{u}, p)$ is the Cauchy stress, which is

$$\boldsymbol{\sigma}(\mathbf{u}, p) = 2\left(\frac{\mu}{\rho}\right)\mathbf{D}(\mathbf{u}) - p\mathbf{I}, \quad (8)$$

where p is the thermodynamic pressure of the fluid, μ is the absolute viscosity of the fluid, ρ is the density of the fluid, **I** is the well-known identity matrix, and $\mathbf{D}(\mathbf{u}) = (\nabla\mathbf{u}+\nabla\mathbf{u}^t)/2$.

The continuous sum is expressed concisely in the weak formulation as follows.

$$a(\boldsymbol{u}, \boldsymbol{u}, \boldsymbol{v}) + b(\boldsymbol{u}, \boldsymbol{v}) - c(\boldsymbol{p}, \boldsymbol{v}) = f(\boldsymbol{v}), \ b(q, \mathbf{u}) = 0. \quad (9)$$

For all $(v, q) \in V \times Q$, we denote the set of solutions $(u, p) \in V \times Q$ as Eq. (9). The functions a, b, c, and f are all continuous, and c satisfies the standard inf-sup condition. According to Oden [8], the existence and uniqueness of the solution of the above equation are available under certain conditions. The a posteriori error estimate of the N-S equation was calculated by considering the equation φ shown below:

$$\mathbf{A}(\boldsymbol{\varphi}, \boldsymbol{v}) + \mathbf{B}(\boldsymbol{\psi}, \boldsymbol{q}) = \mathbf{b}(\boldsymbol{e}, \boldsymbol{v}) - c(\boldsymbol{E}, \boldsymbol{v}) - c(q, \boldsymbol{e}) + a(\boldsymbol{u}, \boldsymbol{u}, \boldsymbol{v}) - a(\boldsymbol{u}^h, \boldsymbol{u}^h, \boldsymbol{v}). \ \forall (\boldsymbol{v}, \boldsymbol{q}) \in \mathbf{V} \times \mathbf{Q}, \ (\boldsymbol{\varphi}, \boldsymbol{\psi}) \in \mathbf{V} \times \mathbf{Q} \quad (10)$$

where $\boldsymbol{e} = \boldsymbol{u} - \boldsymbol{u}^h$, $\boldsymbol{E} = p - p^h$. $\|(\boldsymbol{e}, \boldsymbol{E})\|_*^2 = \mathbf{A}(\boldsymbol{\varphi}, \boldsymbol{\varphi}) + \mathbf{B}(\boldsymbol{\psi}, \boldsymbol{\psi})\mathbf{m}$, u, p is the true solution, u^h, p^h is finite element solutions. Equation (10) is re-written as

$$\mathbf{A}_K(\boldsymbol{\varphi}_K, \mathbf{v}_K) = f_K(\mathbf{v}_K) - b_K(\mathbf{u}_K^h, \mathbf{v}_K) + \mathbf{c}_K(p_K^h, \mathbf{v}_K) - a_K(\mathbf{u}_K^h, \mathbf{u}_K^h, \mathbf{v}_K) + \oint_{\partial\Omega_K} \langle\, \mathbf{n}_K \cdot \boldsymbol{\sigma}(\mathbf{u}^h, p^h) \,\rangle \cdot \mathbf{v}_K ds$$

$$B_K(\Psi_K, q_K) = c_K(q_K, \mathbf{u}_K^h), \tag{11}$$

The above equations are used to obtain the error estimator. However, we only estimated several important areas to reduce the calculation time and increase the convenience of the actual software operation. For time calculation, we used the previous research results [9] as the basis for time difference estimation. Then, COMSOL 5.6 software was used for calculation. The research was based on a relatively reliable computational theory. Calculation results are obtained after detailed estimation in both space and time, and then used as an information source for discussion and research problems.

3. Results and Discussion

To date, it remains challenging by using radiological modalities to reveal in vivo blood flow physical quantities at the transverse-sigmoid junction in depth. To that end, the CFD technique has been an advantageous method to provide hemodynamic perspectives for patients with PT. The vortex generation inside the sigmoid sinus diverticulum has long been considered a source of PT. Therefore, the state of blood flow in this section is considered to be an issue worth exploring. Knowing the preconditions for vortex generation may provide some useful information regarding the causes of PT. Further analysis on surgical procedures addressing diverticular vortex also benefits surgeons in optimizing the therapeutic effect on PT.

In this study, the blood flow is measured every four heartbeat cycles as the reference value of the velocity inlet for the calculation. At each time point, the amount of flow in the vein is converted into a uniform flow velocity in the cross-section of the blood vessel. Fig. 1 demonstrates the inflow velocity value of the flow field, in which four heartbeat cycles are taken into calculation. The proximal end of the transverse sinus was set as the velocity inlet. All branches were removed, and zero pressure was set at the outlet region.

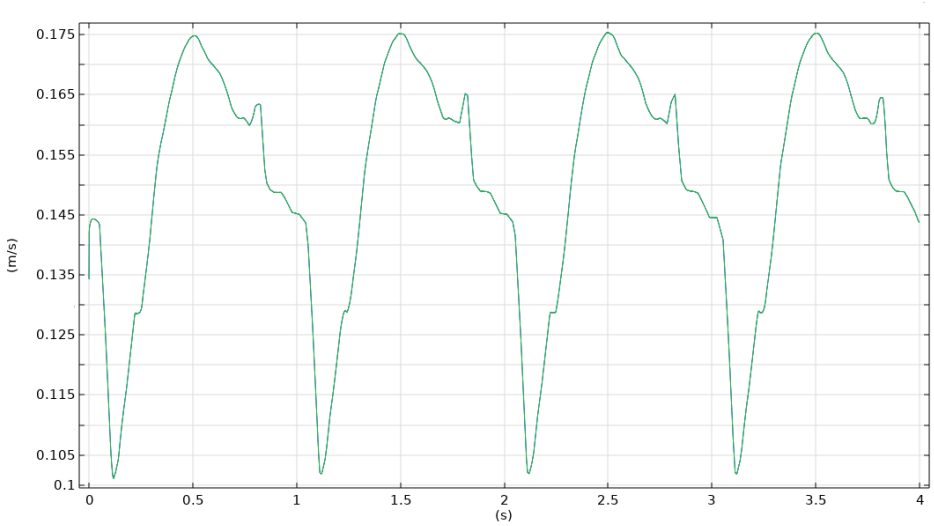

Fig. 1. Mean velocity of blood flow into the sigmoid sinus as a function of four heart cycles.

Fig. 2 shows the streamlined velocity diagram of the flow field at the specific time point (t = 1.5 s) when the blood flow reaches the peak velocity. The color scaling bar on the right represents the velocity of the flow field. According to Fig. 2, there is obvious vortex generation in the flow field, especially near the diverticulum. In this case, the blood flow accelerates and diverts into the diverticulum due to the transverse sinus stenosis, forming a jet flow impinging on the sigmoid sinus wall. In addition, the outpouching contour of the diverticulum gives rise to the vortex generation.

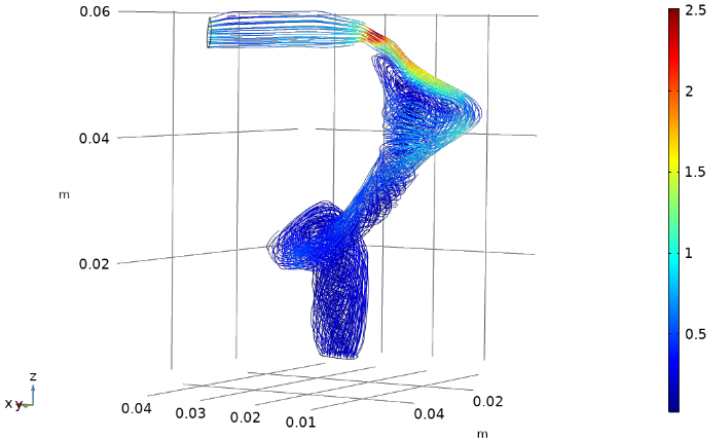

Fig. 2. 3D streamline velocity map of blood flow in the sigmoid sinus at a time of 1.5 s.

Fig. 3 exhibits the vortical flow structure inside the diverticulum using the *XY* cut-plane. It is shown that the vortex velocity is comparatively lower than that of the mainstream sinus flow. Different directions of the vortex likely lead to the deceleration of the intradiverticular blood flow. The end timepoint of vortex development was at t = 0.4 s. Fig. 4 shows the pressure-velocity diagram, in which the arrows represent the direction and magnitude of the flow velocity of the blood flow. The color of the scaling bar represents the magnitude of the pressure, and the pressure unit is Pa. Based on Fig. 4, the diverticular wall pressure is higher than those in other areas. This likely results from the direct impact of the upstream transverse sinus flow. Further studies on the amplitude of the high-velocity vortex are warranted.

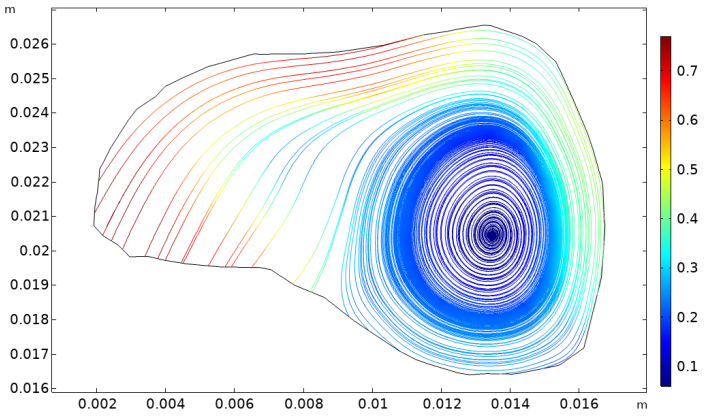

Fig. 3. Streamline velocity diagram in the XY plane near the diverticulum at time = 0.4 s.

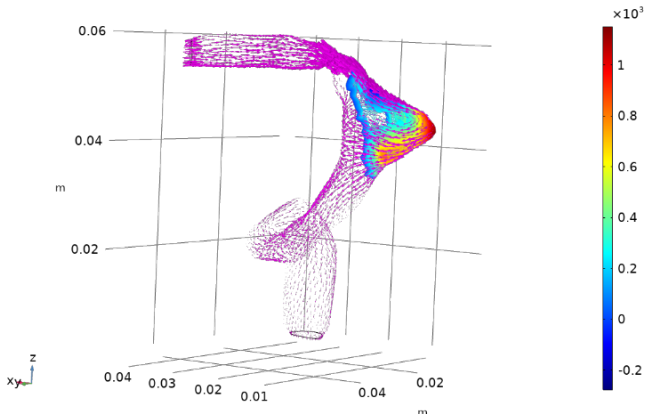

Fig. 4. Distribution of pressure and velocity of blood flow near the diverticulum at time = 1.5 s.

To further understand the mean flow pressure inside the diverticulum, we calculated the average pressure versus time shown in Figs. 4 and 5. The pressure fluctuates twice regularly in one cardiac cycle due to the systole and diastole of the heart. These graphs also show that the average pressure in the diverticulum during cardiac systole can be twice the maximum pressure during diastole.

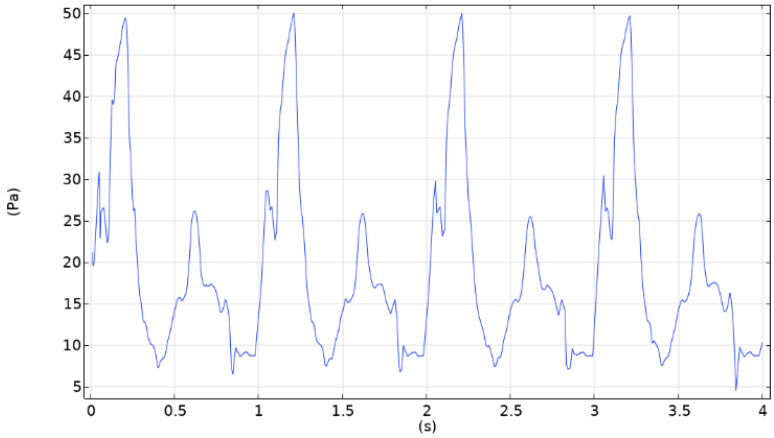

Fig. 5. Mean pressure of blood flow around the diverticulum versus four heartbeat cycles.

The ordinate values in Figs. 6 to 7 are the inertial force ρa($\boldsymbol{u}^h, \boldsymbol{u}^h, \boldsymbol{v}$). The abscissa represents time. Figure 6 exhibits the location where the vortex is generated. Two fixed points are the location where the vortex occurs, where the location is the point where the inertial force is generated as the vortex occurs. Fig. 7 displays the variation of inertial force in the region without a vortex, and is conceptually identical to Fig. 6, except that the selected positions of the two points are at the place without a vortex, the control variable of this study. We chose two points for the convenience of explanation, and the trends of all physical quantities were coherent. However, Figs. 6 and 7 show that the inertial force of the area with vortex fluctuates before vortex generation. The fluctuation of the inertial force is more significant in the region without a vortex. The inertial force of the flow merely altered once in the region without vortex. The reason is likely because the instability of inertial force in the vortex region is higher than in regions without a vortex. In addition, Figs. 6(b) and 7 exhibit the difference between the maximum and minimum inertial force, which is much larger in proportion than the region without a vortex. After 0.4 s (Fig. 6), the fluctuation of the inertial force, both green and blue line, is reduced. This is a steady state after vortex generation. For the magnitude of inertial force, the region where the vortex occurs is much smaller than the region without a vortex. Since the magnitude inertial force is large enough, the ability to maintain the flow inertia is strong. Thus, the consideration to improve the entire flow field to decrease the fluctuation of inertial force is required if the reduction of the diverticular vortex generation is expected. This finding provides a theoretical basis for the development of surgical procedures to further study for a thorough explanation of the refinement of calculation precision.

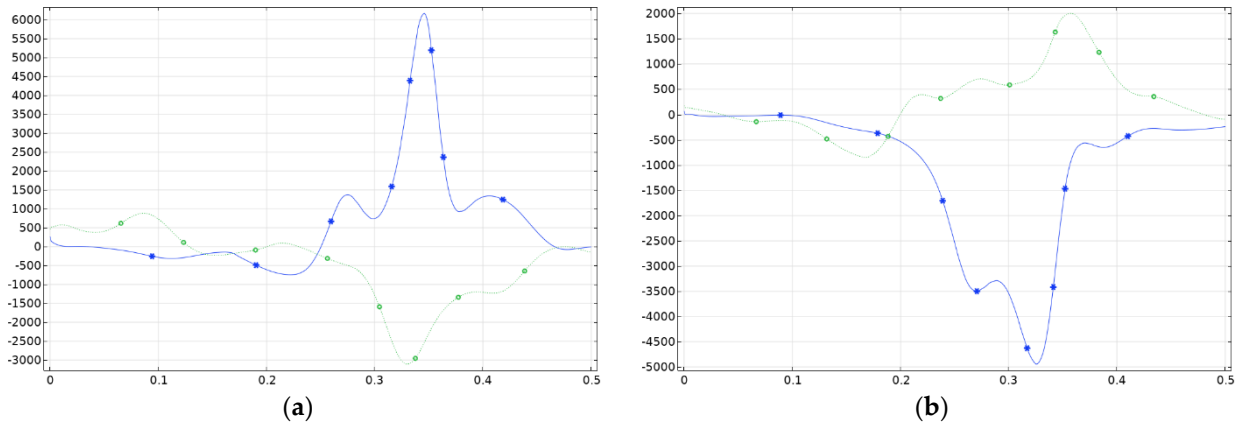

Figure 6. Two points near the center of the vortex of the diverticulum and the jugular bulb region (the two points with the highest and the lowest inertial force) as a function of time. (**a**) The variation of the highest inertial force (blue line, reference point 1) and the lowest inertial force (green line, center point 1) with time near the center of the diverticulum. (**b**) The variation of the highest (green line, center point 2) and the lowest inertial force (blue line, reference point 2) with time near the center of the jugular bulb region.

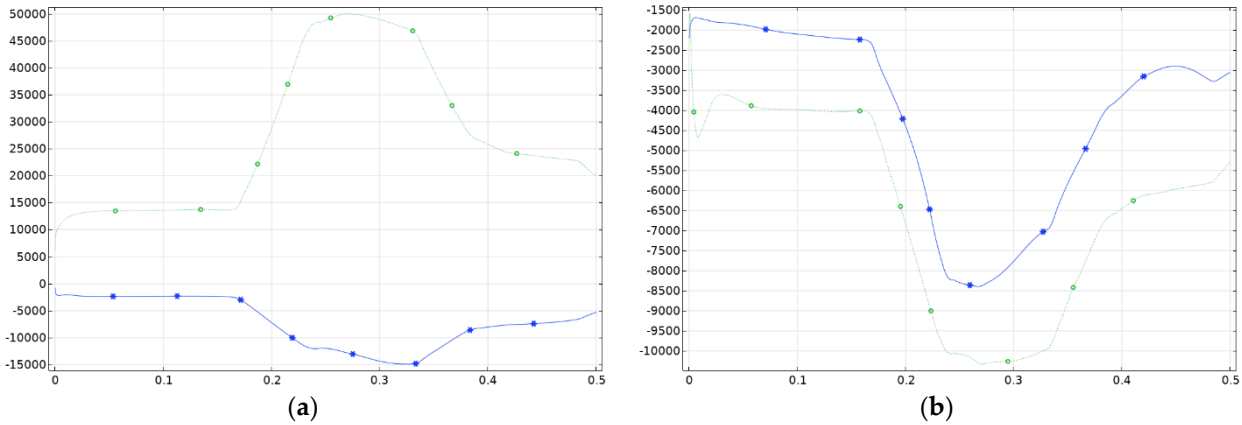

Fig. 7. Fluctuation of the inertial force at two specific points within no vortex region (the selection method of the two points and indicative line colors are the same in Fig. 6) during the same period in the diverticulum region (**a**) and the jugular bulb region (**b**).

The reliability of calculations and results from three perspectives have been discussed in this study: (1) adaptive calculation to space, (2) the adaptive calculation to time, and (3) qualitative comparison of the vortex generation. In addition, the error estimator was calculated, which there was a gradual decrease alongside the successive increase of the degree of freedom (Table 1). This phenomenon is consistent with the results obtained in Ref. [8], which discussed the problem of steady-state pipe flow in two-dimensional space. There was a limitation of this study in terms of dimensions (three-dimensional space transient problem). However, from an engineering point of view, Ref. [8] and this study have consistent convergence effects. Oden et al. [8] mentioned that they adopted three adaptive methods (h, p, and h-p)when they reapplied the philosophical concept of adaptability: h, p, and h-p to carry out numerical experiments. We implemented the concept of adaptive philosophy only for h. Although the methods are different, the convergence is similar to the results obtained by the h strategy in the research.

Table 1. Values of estimated error, velocity, and pressure concerning the degree of freedom of the adaptive mesh.

Mesh	8k	20k	40k	60k	1M	3M
Estimated error	252.11	187.05	201.65	108.91	32.19	15.86
Velocity	0.17	0.22	0.14	0.32	0.36	0.35
Pressure	21.47	49.51	42.38	43.75	41.39	40.81

From the perspective of adaptability to time in the calculation process, we referred to the result obtained by Jeong et al. [10]. Although they used a different method, the actual calculation results can be compared from the perspective of effectiveness. The effectiveness shown by both is comparable as shown in Table 2.

Table 2. Two specific points values of velocity and pressure w.r.t time.

Time (s)	0.01	0.015	0.018	0.02	0.025	0.03	0.036
Velocity 1	0.35	0.34	0.33	0.32	0.32	0.31	0.30
Velocity 2	0.066	0.066	0.065	0.065	0.064	0.063	0.062
Pressure 1	389.69	357.72	346.49	340.40	330.05	324.96	326.92
Pressure 2	322.97	314.36	310.57	309.40	307.81	305.66	311.30

As far as the position of vortex generation is concerned, Hsieh et al. [11] found and established the vortex generation. For the mathematical conditions of regional vortex generation, two physical quantities are usually used to determine,

$$Q = -\frac{1}{2}\mathrm{tr}(\boldsymbol{S}_{ij}^2 + \boldsymbol{\Omega}_{ij}^2) > 0 \quad (12)$$

$$\text{and } \lambda_2 < 0.\ \mathbf{S}_{ij} = \frac{1}{2}(u_{i,j} + u_{j,i}),\ \boldsymbol{\Omega}_{ij} = \frac{1}{2}(u_{i,j} - u_{j,i}) \quad (13)$$

where $\lambda_1 \geq \lambda_2 \geq \lambda_3$ are the eigenvalues of $\boldsymbol{S}_{ij}^2 + \boldsymbol{\Omega}_{ij}^2$, u is generally known to represent the velocity of the fluid, and $u_{i,j}$ is the generally known tensor symbol. In other words, if the location of the vortex generation satisfies the above two conditions, the calculations in this study are confirmed (Table 3).

Table 3. Select three specific points in each region to calculate the Qi and λ2 values before vortex-generation.

Q_i and λ	Q_1	λ_2	Q_2	λ_2	Q_3	λ_2
Point 1	1819.1	-2076.22	967.63	-315.04	3817.6	-323.91
Point 2	-287.42	147.70	-2946.67	2310.0	-2379.9	2347.14
Point 3	-525.41	345.40	-5262.11	3974.92	121.63	-120.38

4. Conclusions

In this research, the sigmoid sinus diverticulum blood flow is studied numerically. The inertial force varied with time and were compared with the cases with or without vortex generation. Changes in intradiverticular vortex hemodynamics with the cardiac cycle were also analyzed. The vortex analysis of sigmoid sinus venous blood flow provides a clue for the pathophysiological study of venous PT. The location of the vortex generation explains the geometry of the vessels causing vortex generation. For the vortex generation, the fluctuation of the inertial force was higher inside the flow field. This shows that the instability of the fluid flow increases before the generation of a vortex. After a vortex generates and remains, the inertial force keeps changing as the state of the fluid motion does not alter. In addition, before a vortex generates, the difference of the inertial force near the vortex is significantly larger than in the area without a vortex. In the same flow field, regions with relatively large fluctuation of the inertial force and relatively small inertial force are more likely to engender vortex. This finding is referred to as the indication of vortex reduction. Regardless of adaptive space or time, the findings in this study per se are used to enhance the computational efficiency and accuracy.

Author Contributions: The authors confirm contributions to the paper as follows: conceptualization, Hsieh and Lin; methodology, Hsieh and Lin; software, Lin; validation, Hsieh; formal analysis, Hsieh; investigation, Hsieh and Lin; resources, Hsieh and Lin; data curation, Hsieh; writing—original draft preparation, Hsieh and Lin; writing—review and editing, Hsieh; visualization, Lin; supervision, Hsieh. Authorship is limited to those who have contributed substantially to the work reported.

Funding: This research did not receive external funding.

Conflicts of Interest: The authors declare no conflict of interest.

References

1. Kim, S.H.; An, G.S.; Choi, I.; Koo, J.W.; Lee, K., Song, J.J. Pre-Treatment Objective Diagnosis and Post-Treatment Outcome Evaluation in Patients with Vascular Pulsatile Tinnitus Using Transcanal Recording and Spectro-Temporal Analysis. *PLoS ONE* **2016**, *11*, e0157722.
2. Eisenman, D.J.; Raghavan, P.; Hertzano, R.; Morales, R. Evaluation and treatment of pulsatile tinnitus associated with sigmoid sinus wall anomalies. *Laryngoscope* **2018**, *128*, S1–S13.
3. Wang, G.-P.; Zeng, R.; Liu, Z.-H.; et al. Clinical characteristics of pulsatile tinnitus caused by sigmoid sinus diverticulum and wall dehiscence: a study of 54 patients. *Acta Otolaryngol*. **2014**, *134*, 7–13.
4. Mattox, D.E.; Hudgins, P. Algorithm for evaluation of pulsatile tinnitus. *Acta Otolaryngol*. **2008**, *128*, 427–431.
5. Liu, G.S.; Boursiquot, B.C.; Blevins, N.H.; Vaisbuch, Y. Systematic review of temporal bone-resurfacing techniques for pulsatile tinnitus associated with vascular wall anomalies. *Otolaryngol Head Neck Surg*. **2019**, *160*, 749–761.
6. Tian, S., Fan, X.,Wang, Y., Liu, Z.; Wang, L. An In Vitro Experimental Study on the Relationship Between Pulsatile Tinnitus and the Dehiscence/ Thinness of Sigmoid Sinus Cortical Plate. *J. Biomech*. **2019**, *84*, 197–203. https://doi.org/10.1016/ j.jbiomech.2018.12.049
7. Hsieh, Y.-L.; Wang, W. Extraluminal Sigmoid Sinus Angioplasty: a Pertinent Reconstructive Surgical Method Targeting Dural Sinus Hemodynamics to Resolve Pulsatile Tinnitus. *Otol. Neurotol*. **2020**, *41*, e132–e145. https://doi.org/10.1097/MAO.0000000000002464
8. Oden, J.; Wu, W.; Ainsworth, M. An a posterior error estimate for finite element approximations of the Navier-Stokes equations. *Computer Methods in Applied Mechanics and Engineering* **1994**, *111*, 185–202.
9. Kay, D..A.; Gresho, P.M.; Griffiths, D.F.; Silvester, D.J. Adaptive Time-Stepping for Incompressible Flow Part II: Navier-Stokes Equations. *SIAM J. Sci. Comput*. **2010**, *32*, 111–128.

10. Jeong, J.; Hussain, F. On the identification of a vortex. *J. Fluid Mech*. **1995**, *285*, 69–94.
11. Hsieh, Y.L.; Hsieh, Y.C.; Han, Z.; Lin, H.F. Microsyst. *Technol*. **2021**, *27*, 1559.